IAHR AIRH
Taylor & Francis
Taylor & Francis Group

Journal of Hydraulic Research Vol. 53, No. 2 (2015), pp. 264–273
http://dx.doi.org/10.1080/00221686.2014.989458

Research paper

Physical modelling of breaking tidal bores: comparison with prototype data

HUBERT CHANSON (IAHR Member), Professor, *School of Civil Engineering, The University of Queensland, Brisbane, Australia*
Email: h.chanson@uq.edu.au (author for correspondence)

YIT-HAW TOI, Research Student, *School of Civil Engineering, The University of Queensland, Brisbane, Australia*

ABSTRACT
A tidal bore is a hydraulic jump in translation, propagating upstream as the tide turns to rising and the flood flow advances in a funnel-shaped river mouth under spring tide conditions. This study focused on the unsteady turbulence induced by a breaking tidal bore. Detailed free-surface and velocity measurements were conducted with a high temporal resolution using non-intrusive free-surface measurement probes and acoustic Doppler velocimetry sampled at 200 Hz. The laboratory data were systematically compared with an earlier series of field measurements conducted in the breaking bore of the Sélune River (France). Key findings include the agreement, in terms of dimensionless instantaneous free-surface and velocity data, between laboratory and field observations as well as the existence of a transient recirculation region near the bed.

Keywords: Breaking tidal bores; physical modelling; prototype-model comparisons; self-similarity; Sélune River; transient recirculation; turbulence

1 Introduction

A tidal bore is a surge of water propagating upstream as the tidal flow turns to rising and the flood tide rushes into a funnel-shaped river mouth of shallow water (Barré de Saint Venant, 1871). The bore forms during the spring tides when the tidal range exceeds 4–6 m and the estuary bathymetry amplifies the tidal range with a low freshwater level (Tricker, 1965). A tidal bore is a front with a sharp discontinuity in water depth (Fig. 1) and its upstream propagation impacts significantly on the ecology of the natural river system (Chanson, 2011). The strength of the bore is typically characterized by its Froude number (defined below). For a Froude number less than 1.5–1.8, the bore is undular: its front is followed by a train of secondary waves called undulations. At larger Froude numbers, the bore front is characterized by a marked roller, i.e. a breaking bore (Fig. 1). Surprisingly, field studies remain limited despite a few successful ones (Chanson, Reungoat, Simon, & Lubin, 2011; Mouazé, Chanson, & Simon, 2010; Reungoat, Chanson, & Caplain, 2014; Simpson, Fisher, & Wiles, 2004).

In this paper, the unsteady turbulence and turbulent mixing induced by a breaking tidal bore are documented based upon new laboratory experiments. The experimental results are then compared systematically with a recent field data set.

2 Physical modelling and methodology

Experimental investigations may provide some detailed information on physical processes, and some recent progress in instrumentation offers the means for successful turbulence measurement in unsteady open channel flows (Hornung, Willert, & Turner, 1995; Koch & Chanson, 2009). For a tidal bore propagating in a horizontal channel, a simplified dimensional analysis yields a series of relationships between the dimensionless flow properties at a given location (x, y, z) at time t as functions of a number of relevant dimensionless numbers characterizing the fluid properties and physical constants, the channel geometry, and the initial and boundary conditions:

$$\frac{P}{\rho\, g\, d_1}, \frac{V_x}{V_1}, \frac{V_y}{V_1}, \frac{V_z}{V_1}, \frac{v_x'}{V_1}, \frac{v_y'}{V_1}, \frac{v_z'}{V_1}, T_{vx}\sqrt{\frac{g}{d_1}}, T_{vy}\sqrt{\frac{g}{d_1}}, T_{vz}\sqrt{\frac{g}{d_1}} \ldots = f\left(\frac{x}{d_1}, \frac{y}{d_1}, \frac{z}{d_1}, t\sqrt{\frac{g}{d_1}}, \frac{V_1+U}{\sqrt{g\, d_1}}, \frac{v_1'}{V_1}, \rho\frac{(V_1+U)\, d_1}{\mu}, \frac{B}{d_1}, \frac{g\,\mu^4}{\rho\,\sigma^3}, \ldots\right) \quad (1)$$

where P is pressure, V, v' and T_v are respectively the instantaneous mean velocity component, root mean square of velocity fluctuation and integral time scale, the subscripts x, y and z refer to the longitudinal, transverse and vertical velocity components,

Received 27 March 2014; accepted 12 November 2014/Open for discussion until 29 Oct 2015.

ISSN 0022-1686 print/ISSN 1814-2079 online
http://www.tandfonline.com

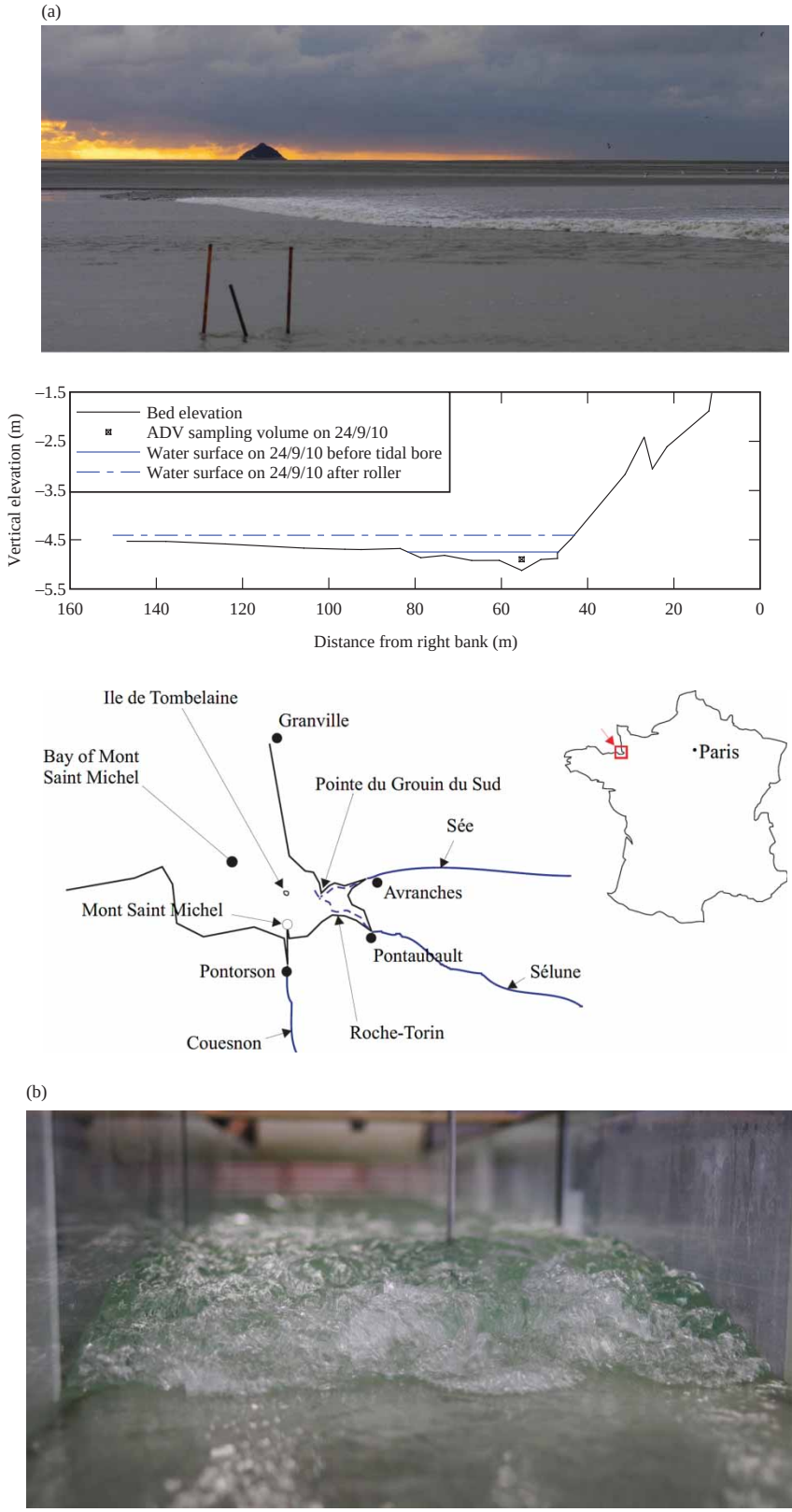

Figure 1 Propagation of breaking tidal bores. (a) Tidal bore of the Sélune River (France) on 24 September 2010 evening, $F_1 = 2.35$, $d_1 = 0.375$ m, $B_1 = 35$ m, $U = 2$ m s^{-1}; top: photograph of the bore advancing (from right to left) with the ADV support in the foreground, middle: surveyed channel cross-section looking downstream, bottom: map of the Bay of Mont Saint Michel (France). (b) Laboratory experiment, looking downstream at the incoming bore roller; $F_1 = 2.1$, $d_1 = 0.0542$ m, $B_1 = 0.5$ m, $U = 0.46$ m s^{-1}

U is the bore celerity positive upstream, d_1 is the initial depth, V_1 is the cross-sectional averaged initial velocity positive downstream, v_1' is the root mean square of velocity fluctuation in the initially steady flow, B is the channel width, g is gravity acceleration, ρ and μ are the water density and dynamic viscosity respectively, and σ is the surface tension between air and water. The fifth and seventh terms on the right-hand side of Eq. 1 are the tidal bore Froude and Reynolds numbers respectively, and the ninth term is the Morton number, a function only of fluid properties and the gravity constant. Note that in Eq. 1 the left-hand side includes only an incomplete characterization of the unsteady flow turbulence, while the right-hand side does not account for the effects of surfactants, biochemicals, sediments and aquatic life, which are relevant in a natural system.

A true dynamic similarity is achieved in a geometrically similar model if and only if each dimensionless term (i.e. Π-term) has the same value in the model and the prototype. Scale effects might occur when one or more Π-terms have different values in the laboratory and in the field. In a tidal bore, the gravity effects are important and a Froude similitude is commonly used (Liggett, 1994; Tricker, 1965). The turbulent mixing processes involve some viscous dissipation, thus implying a Reynolds similitude. It is, however, impossible to satisfy simultaneously a true dynamic similarity in geometrically similar models with the same fluids in the model and the prototype. In the present study, both Froude and Morton similitudes were adopted following Hornung et al. (1995) and Koch & Chanson (2009). The laboratory results (presented below) were systematically compared with some field measurements recently conducted in breaking tidal bores (Mouazé et al., 2010). That field study was conducted in the Bay of Mont Saint Michel, France. Figure 1a presents a photograph of the bore, the surveyed channel cross-section and a map of the sampling site. Further details are summarized in Table 1.

The laboratory experiments were performed in a 12 m long 0.5 m wide tilting flume previously used by Koch & Chanson (2009), but with different flow conditions (Table 1, Fig. 1b). The channel bed was made of smooth PVC and the sidewalls were glass panels. The unsteady water depth was measured with several acoustic displacement meters, Microsonic Mic + 25/IU/TC, located above the channel centreline. The free-surface measurements were repeated 25 times and ensemble-averaged. The velocity measurements were performed using an acoustic Doppler velocimeter (ADV) Nortek Vectrino +. The ADV sampling volume was located at $x = 4.5$ m on the flume centreline, with $x = 0$ at the upstream end of the flume. The ADV sampling volume was positioned beneath the free-surface prior to the tidal bore: $z/d_1 < 0.9$. During the tidal bore passage, visual observations through the glass sidewalls showed that the entrained air bubbles were rapidly advected upwards by buoyancy effects and no air bubble was seen deeper than $z/d_1 = 1$. Thus, the ADV signal was unaffected by entrained bubbles. The ADV and displacement sensors were sampled simultaneously at 200 Hz.

A fast-closing Tainter gate located at $x = 11.15$ m was used to generate a tidal bore propagating upstream against the initially steady flow. The experimental flow conditions encompassed both breaking and undular bores, all generated with the same initial flow rate, although the velocity measurements were conducted in breaking bores only (Table 1). It is acknowledged that the laboratory conditions did not cover the same range of Froude numbers as the prototype data (Mouazé et al., 2010). This was a limitation inherent in the experimental facility, as visual observations showed that the wake behind the ADV stem became large and affected the incoming bore for Froude numbers greater than 2.2. The experimental flow conditions were selected to cover a relatively broad range of breaking bore Froude numbers (1.7–2.1), thus enabling a check for data consistency and trend.

3 Basic observations

The tidal bore shape was closely linked with its Froude number:

$$\mathrm{F}_1 = \frac{V_1 + U}{\sqrt{g \frac{A_1}{B_1}}} \tag{2}$$

where A and B are respectively the flow cross-section area and free-surface width, and the subscript 1 refers to the initial flow conditions. For Froude numbers less than 1.5–1.7, an undular bore was observed. The bore front was followed by a train of pseudo-periodic undulations. For tidal bores with Froude numbers greater than 1.7, a breaking bore front was seen, with a marked roller extending across the whole channel width (Fig. 1b). A key feature was the flow singularity at the roller toe where air bubbles were entrained and vorticity was generated. Some air entrainment and intense turbulent mixing were observed in the bore roller, with increasing mixing and air entrapment with increasing Froude number. Overall the visual observations were consistent with earlier observations (Benet & Cunge, 1971; Hornung et al., 1995; Koch & Chanson, 2009). The flow properties immediately before and after the tidal bore front had to satisfy the continuity and momentum principles (Liggett, 1994; Chanson, 2012). For a one-dimensional flow motion, the integral form of mass and momentum conservations gives a series of relationships between the flow properties in front of and behind the bore front:

$$\frac{A_2}{A_1} = \frac{1}{2} \frac{\sqrt{\left(2 - \frac{B'}{B}\right)^2 + 8 \frac{\frac{B'}{B}}{\frac{B_1}{B}} \mathrm{F}_1^2} - \left(2 - \frac{B'}{B}\right)}{\frac{B'}{B}} \tag{3}$$

where the subscript 2 refers to the flow conditions immediately after the jump (Chanson, 2012), while B and B' are characteristic

Table 1 Details of turbulent velocity measurements in breaking tidal bores: field and laboratory studies

Reference	Q (m^3 s^{-1})	S_o	Bed roughness	d_1 (m)	V_1 (m s^{-1})	V_2 (m s^{-1})	U (m s^{-1})	F_1	$\rho \frac{(V_1 + U)\, d_1}{\mu}$	Site	Date (m)	Instrumentation
(1)	(2)	(3)	(4)	(5)	(6)	(7)	(8)	(9)	(10)	(11)	(12)	(13)
Field studies												
Simpson et al. (2004)	N/A	N/A	Mobile bed & bed forms	0.72	0.15	− 1.1	4.1	1.8	3.0×10^6	Dee River (UK)	6/9/03	ADCP. Sampling: 10 Hz.
Mouazé et al. (2010)	N/A	N/A	Mobile bed (’*tangue*’)	0.375	0.86	− 0.95	2.0	2.35	1.1×10^6	Sélune River (France)	24/9/10	ADV Vector.
				0.325	0.59	− 1.20	1.96	2.48	8.2×10^5		25/9/10	Sampling: 64 Hz
Laboratory studies												
Koch & Chanson (2009)	0.040	0	Smooth PVC	0.079	1.01	–	0.541	1.77	1.2×10^5	Laboratory	N/A	MicroADV. Sampling: 50 Hz
Chanson (2010)	0.058	0	Smooth PVC	0.139	0.832	0.14	0.903	1.50	2.4×10^5	Laboratory	N/A	ADV Vectrino +.
			Rough screen (k_s = 6.6 mm)	0.141	0.824	0.16	0.892	1.46	2.4×10^5			Sampling: 200 Hz
Chanson & Docherty (2012)	0.050	0.0	Smooth PVC	0.118	0.848	0.081	0.867	1.59	2.0×10^5	Laboratory	N/A	ADV Vectrino +.
		0.002	Fixed gravel (k_s = 3.4 mm)	0.126	0.794	0.13	0.866	1.49	2.1×10^5			Sampling: 200 Hz
Current study	0.025	0.0035	Smooth PVC	0.0517	0.966	0.07	0.529	2.10	7.7×10^4	Laboratory	N/A	ADV Vectrino +.
				0.0514	0.973	0.13	0.462	2.02	7.3×10^4			Sampling: 200 Hz
				0.0519	0.963	0.21	0.398	1.91	7.0×10^4			
				0.0508	0.973	0.35	0.263	1.74	6.2×10^4			

Notes: Q: initial steady flow rate; S_o: bed slope; d_1, V_1: initial flow depth and velocity recorded at sampling location; U: tidal bore celerity positive upstream on the channel centreline; F_1: tidal bore Froude number (Eq. 2).

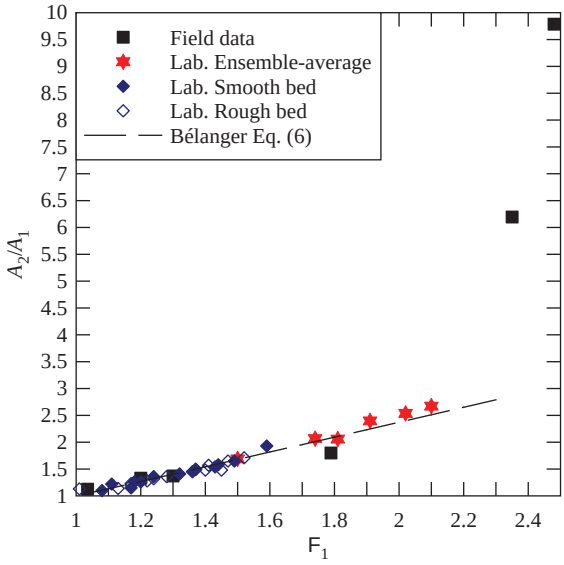

Figure 2 Ratio of conjugate cross-section areas A_2/A_1 as a function of the bore Froude number F_1; comparison between field data, laboratory data (ensemble-averaged: Chanson & Docherty, 2012; current study; single data set: Chanson, 2010; Chanson & Docherty, 2012) and the Bélanger equation (Eq. 4)

channel widths:

$$B = \frac{A_2 - A_1}{d_2 - d_1} \tag{4}$$

$$B' = \frac{\int_{A_1}^{A_2} \int \rho g \, (d_2 - y) \, dA}{\frac{1}{2} \rho g \, (d_2 - d_1)^2} \tag{5}$$

For a bore in a rectangular prismatic channel, Eq. 3 simplifies into the Bélanger equation:

$$\frac{d_2}{d_1} = \frac{1}{2} \left(\sqrt{1 + 8 \, F_1^2} - 1 \right) \tag{6}$$

where d is the flow depth. The ratio of conjugate cross-sections areas A_2/A_1 at $x = 4.5$ m is presented as a function of the Froude number in Fig. 2, with the present data being ensemble-averaged over 25 experiments. The results showed a good agreement with a range of laboratory and field data, but for a couple of data points (Fig. 2, top right) being the Sélune River bore. At that sampling site, the channel cross-section was not rectangular and its left bank was a shallow sand flat. The advancing bore front expanded in the transverse direction: "The tidal bore front has a curved shape. [...] On the left bank, the bore front advanced on the dry sand bank" (Mouazé et al., 2010). The assumption of one-dimensional flow was not valid and the channel cross-section was not rectangular, thus restricting the application of Eq. 6. Overall, Fig. 2 showed a good agreement between theory and data, and the result was irrespective of the bed roughness in the laboratory.

Some typical instantaneous free-surface data are presented in Fig. 3. Both field and laboratory measurements are shown and the origin of the horizontal axis is the passage of the roller toe ($t = T_{toe}$). The data showed time-variations of bore roller height that were very close to photographic observations. The results in terms of roller length are summarized in Fig. 4a, in which the tidal bore data are compared with stationary hydraulic jump data. Herein, the bore roller length was equivalent to the bore celerity U times the roller duration T_{roller}. The comparison (Fig. 4a) shows the agreement between laboratory data of a stationary hydraulic jump and a hydraulic jump in translation. The time-variations of the roller free-surface elevation presented a self-similar profile (Fig. 4b):

$$\frac{d - d_1}{d_2 - d_1} = \left(\frac{t - T_{toe}}{T_{roller}} \right)^{0.6} \tag{7}$$

where T_{roller} is the duration of the breaking roller past the sampling point. The bore roller profile data compared favourably with the theoretical models of Valiani (1997) and Richards & Gavrilyuk (2013).

The velocity data indicated the marked impact of the breaking bore propagation (Fig. 3). Figure 3 shows the time-variations of the longitudinal velocity at several vertical elevations during the bore passage, where V_2 is the conjugate flow velocity. The bore propagation was associated with a sudden rise in free surface elevation and a sharp flow deceleration. The laboratory instantaneous velocity measurements (Fig. 3a) presented a comparable trend to the field data in the Sélune River (Fig. 3b) for a similar relative elevation z/d_1. The tidal bore passage was linked with large fluctuations of all three velocity components during the tidal bore and during the early flood tide. The magnitude of the flow deceleration was quantified in terms of the maximum longitudinal deceleration, calculated based upon the low-pass filtered velocity signal (Fig. 5). Figure 5 summarizes the vertical distributions of maximum deceleration. On average, the deceleration was 0.14 g in the laboratory, compared with a maximum deceleration of about 0.16 g in the Sélune River.

A key feature of the breaking bores was the existence of some transient recirculation close to the bed immediately behind the roller. The recirculation is sketched in Fig. 6a and highlighted in Fig. 3. The amplitude of maximum recirculation velocity decreased with increasing distance from the channel bed. The characteristics of the transient recirculation region were derived from the velocity data collected at several vertical elevations. The current data show that the dimensions of transient recirculation region (Fig. 6b) and the maximum recirculation velocity amplitude both increased with increasing Froude number. The maximum recirculation velocity and the duration of the transient recirculation data are regrouped in Figs. 6c and 6d respectively. The maximum recirculation was typically observed shortly after the bore roller in the laboratory. The field data in the Sélune River indicated a comparatively stronger recirculation transient (Fig. 6c) and longer recirculation zone (Fig. 6d). This might be linked to the irregular channel bathymetry as well as to changes in the movable boundaries during the bore advance.

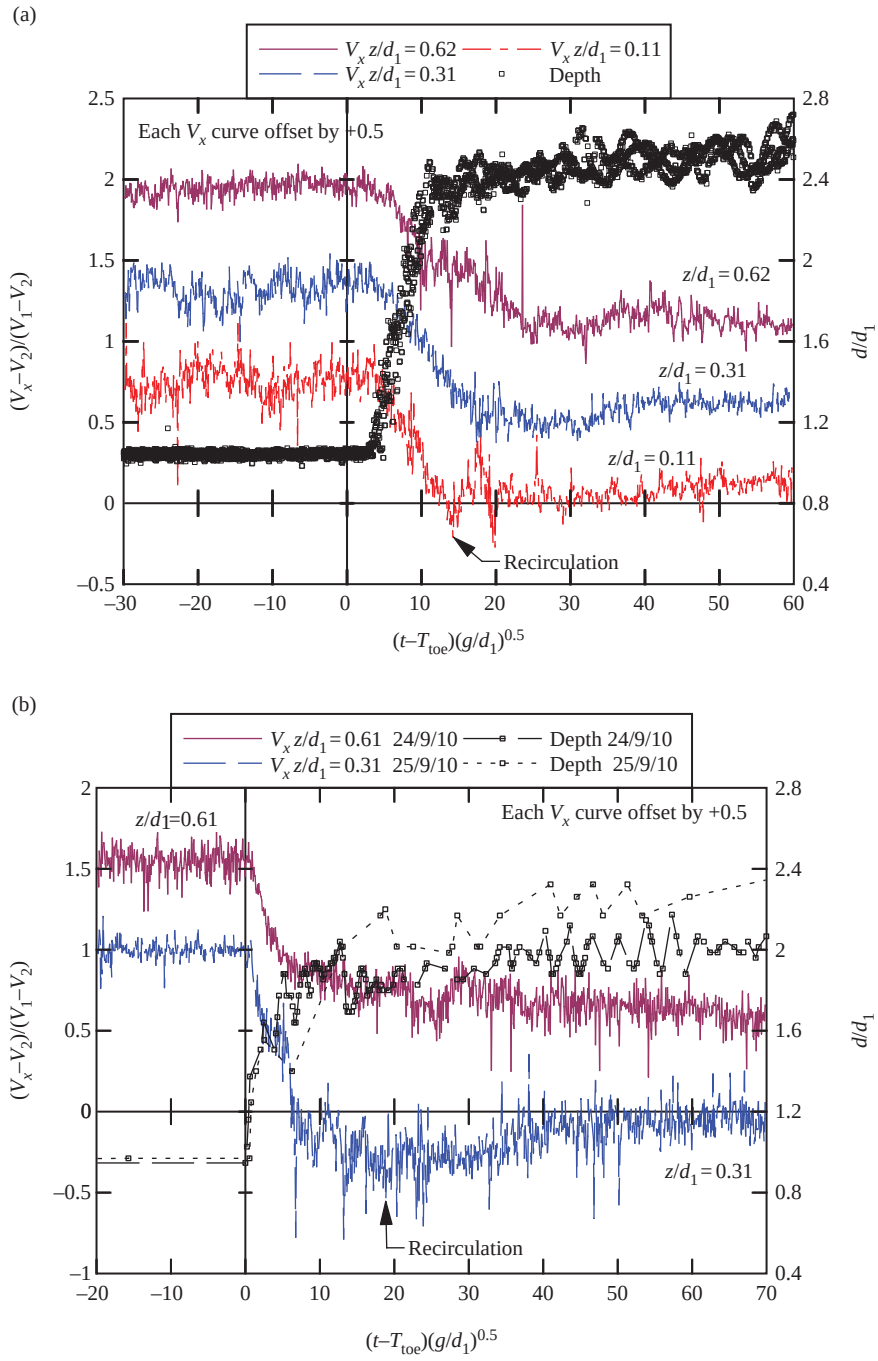

Figure 3 Dimensionless water depth and longitudinal velocity measurements in breaking tidal bores in laboratory (current study) and in the field (Mouazé et al., 2010). Each longitudinal velocity curve is offset vertically by +0.5 from the previous one (colour figures available online). (a) Laboratory data, $d_1 = 0.0514$ m, $F_1 = 2.02$. (b) Field data in the Sélune River, $d_1 = 0.325$ m, $F_1 \approx 2.4$

In the Sélune River, the river bed consisted of a mixture of non-cohesive and cohesive sediment materials, locally known as "*tangue*" (Tessier, et al., 1995). During the installation and removal of the instrumentation, the people in the water (including the first author) felt the sediment motion during the late ebb tide, in the form of particles impacting the legs and submerged body of the individuals. With the incoming tidal bore, intense sediment motion, including scour and advection, was observed in the tidal bore roller, and this was clearly seen next to the banks (Mouazé et al., 2010).

Some characteristic turbulent time scales were derived from the instantaneous velocity data. The integral time scale T_v, also called the Eulerian integral time scale, was calculated as (Hinze 1975):

$$T_v = \int_{\tau=0}^{\tau(R_{xx}=0)} R_{xx} \mathrm{d}\tau \tag{8}$$

where τ is the time lag, and R_{xx} is the normalized auto-correlation function of the turbulent velocity fluctuation v from

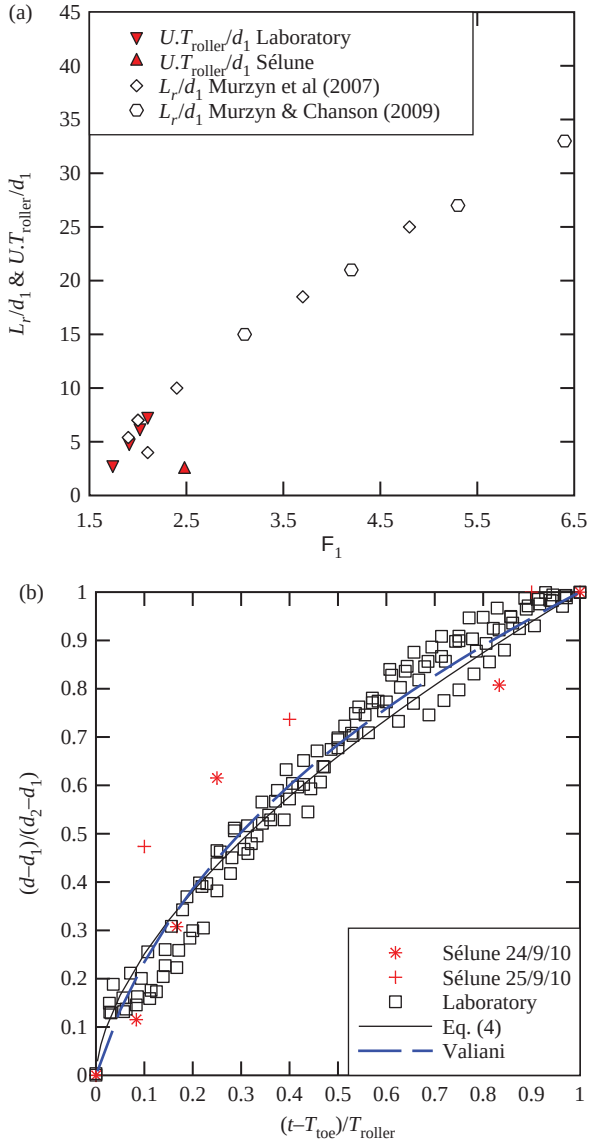

Figure 4 Dimensionless properties of breaking tidal bores. (a) Dimensionless roller length in breaking tidal bores; comparison between prototype data (Sélune River, Mouazé et al., 2010), laboratory data (current study) and stationary hydraulic jump data (Murzyn, Mouazé, & Chaplin, 2007; Murzyn & Chanson, 2009). (b) Self-similar free–surface profiles in breaking tidal bores; comparison between prototype data (Sélune River, Mouazé et al., 2010), ensemble-averaged laboratory data (present study), Eq. 7, and the theoretical solution of Valiani (1997) for $F_1 = 2.1$

a mean trend and defined as:

$$R_{xx}(\tau) = \frac{\int_{t=0}^{T} v(t)\ v(t+\tau)\ dt}{\left(\int_{t=0}^{T} v(t)\ dt\right)^2} \quad (9)$$

with an integration time T significantly longer than the integral turbulent time scale T_v but smaller than the hydrodynamic time scale. Based upon a sensitivity analysis conducted for $0.5 < T < 10$ s, $T = 2$ s was used for both laboratory and field data

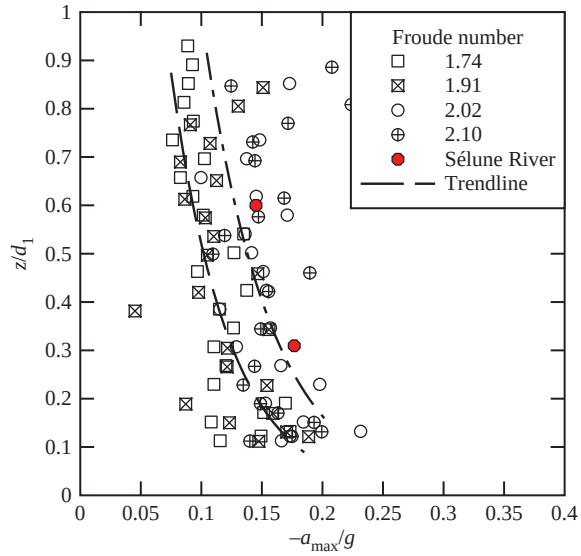

Figure 5 Dimensionless longitudinal deceleration in breaking tidal bores; comparison between prototype data (Sélune River, Mouazé et al., 2010) and laboratory data (current study). Trendlines for $F_1 = 1.74$ (left) and 2.1 (left)

because little difference was observed for $T \geq 2$ s. The data indicated that, in the laboratory, the dimensionless integral time scales $T_v(g/d_1)^{1/2}$ were about 0.2–0.25 for the horizontal and transverse velocity components, and 0.08–0.1 for the vertical velocity component. The approximate factor of two between the longitudinal and vertical velocity time scales agreed with the analytical relation for isotropic turbulence (Hinze, 1975), while the unity ratio between longitudinal and transverse time scales might reflect some turbulence anisotropy. In the Sélune River, the dimensionless integral time scales were about 0.1–0.12 for the horizontal velocity component, and between 0.04 and 0.06 for the transverse and vertical velocity components. Since the turbulent eddies most closely associated with the integral time scales are the energy-containing eddies (Lewalle & Ashpis, 2004), the findings suggested that the turbulent energy was contained in short-lived small-scale vortical structures.

4 Discussion

The comparison between laboratory and field data presented some differences in terms of the initially-steady flow conditions. In the Sélune River on 24 September 2010, the initial river flow was transcritical and some small free-surface standing waves were seen. At the sampling elevation $z/d_1 = 0.6$, the time-averaged longitudinal velocity V_x equalled $+0.98$ m s^{-1}, and the dimensionless velocity standard deviations were: $v_x'/V_x = 0.16$, $v_y'/V_x = 0.04$, and $v_z'/V_x = 0.14$. For comparison, the present laboratory study yielded the following initially steady flow conditions: $V_x = +1.08$ m s^{-1}, $v_x'/V_x = 0.068$, $v_y'/V_x = 0.032$, and $v_z'/V_x = 0.12$ at $z/d_1 = 0.6$. Despite these differences in initial conditions and the movable boundaries of the Sélune River channel, the present comparative analysis showed

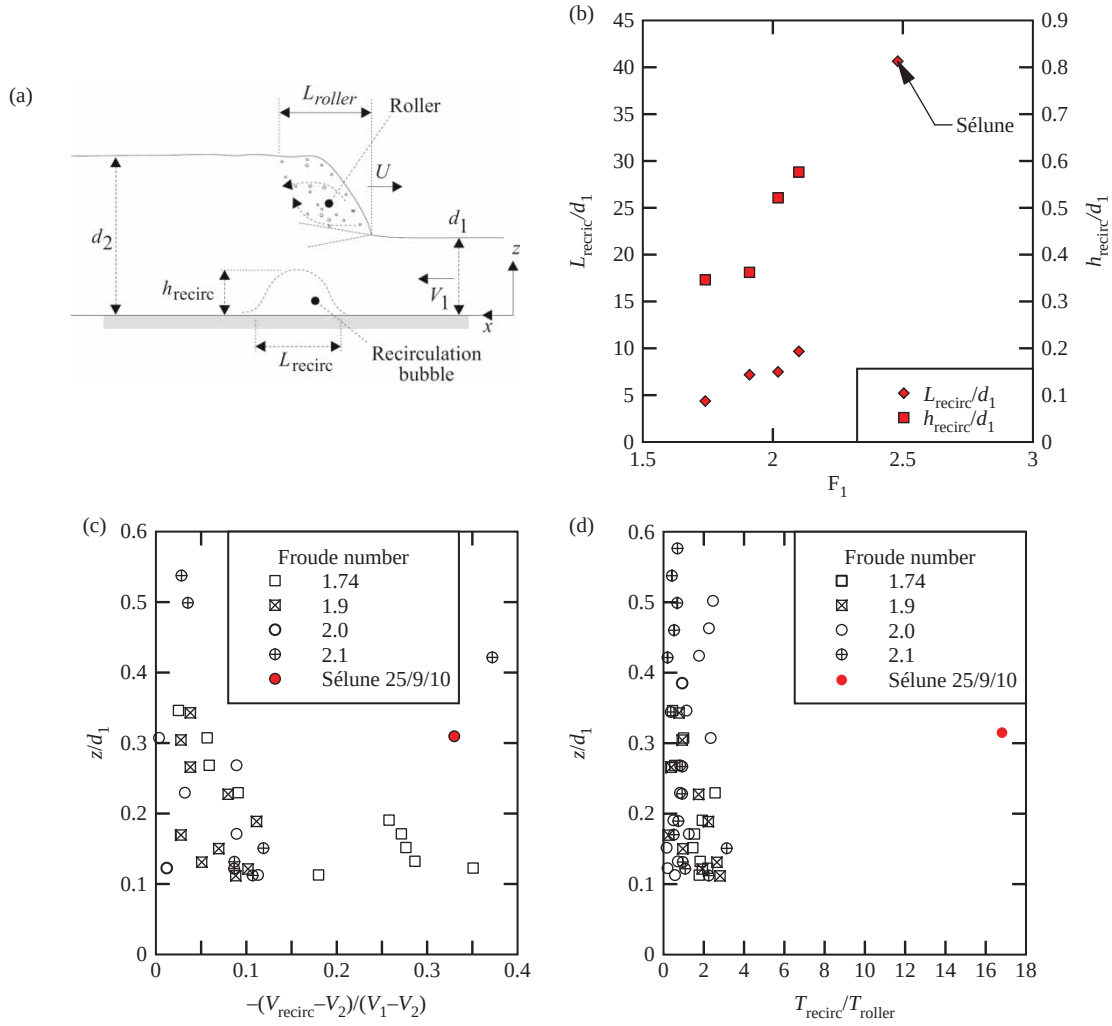

Figure 6 Transient recirculation characteristics beneath breaking tidal bores. (a) Definition sketch. (b) Dimensionless recirculation region length and height in breaking tidal bores; comparison between prototype data (Sélune River, Mouazé et al., 2010) and laboratory data (current study). (c) Dimensionless maximum recirculation velocity in the recirculation bubble. (d) Dimensionless duration of the transient recirculation

some close agreement in terms of dimensionless instantaneous free-surface and velocity data, and integral turbulent time scales, between laboratory and field observations. The finding is important because it supports the correct similitude of the macro-scale turbulence in the physical model. Relatively large-size laboratory models simulate well the features of the unsteady turbulent flow.

In some recent experiments of breaking bores above a movable bed conducted for $F_1 = 1.4$ (Khezri & Chanson, 2012), the median maximum particle acceleration was 0.4 g with 10% of particles experiencing longitudinal acceleration in excess of 1 g. These acceleration levels were significantly larger than the flow deceleration measurements (see above). The finding might indicate the predominant role of the longitudinal pressure gradient to destabilize and accelerate the sediment particles.

5 Conclusions

The study reported in this paper has focused on the unsteady turbulence induced by a breaking tidal bore. Detailed free-surface and velocity measurements were performed with a high-temporal resolution using non-intrusive free-surface measurement probes and side-looking acoustic Doppler velocimetry in a relatively large channel. The laboratory data were compared systematically with field measurements conducted in the breaking bore of the Sélune River (France) by Mouazé et al. (2010). The propagation of a breaking tidal bore was associated with a sharp free-surface discontinuity at the bore front, followed by some transient recirculation next to the bed. The field data indicated a comparatively stronger recirculation transient and longer recirculation zone, which might be linked with changes in the movable boundaries during the bore advance.

The flow properties upstream and downstream of the bore front fulfilled basic momentum considerations. The roller surface presented a self-similar profile close to classical stationary hydraulic jump results. The propagation of the bore was associated with a sudden flow deceleration at all vertical elevations. A key finding was the general agreement in terms of dimensionless instantaneous free-surface and velocity data between laboratory and field observations. To the best of our knowledge,

such a model-prototype comparison has never been tested for tidal bores to that level to date. Field conditions are typically characterized by an active mobile bed, some sediment processes and an irregular channel cross-section, and these effects might need to be taken into account in future works.

Acknowledgements

The first writer acknowledges the assistance of his former students Mr Chu Cheng (Adrian) Yao and Pei Yuan Yeo, and Ms Winnie Man, as well as the technical assistance of Ahmed Ibrahim and Jason Van Der Gevel (The University of Queensland). He further thanks Professor Colin Apelt (The University of Queensland) for his valuable suggestions.

Notation

A = cross-section area (m^2)
A_1 = inflow cross-section area (m^2)
A_2 = conjugate cross-section area (m^2)
a = acceleration (m s^{-2})
a_{max} = maximum deceleration (m s^{-2})
B = channel width (m)
B' = characteristic channel width (m)
B_1 = inflow free-surface width (m)
d = water depth (m)
d_1 = inflow depth (m)
d_2 = conjugate flow depth (m)
F_1 = inflow Froude number (–)
g = gravity acceleration (m s^{-2})
h_{recirc} = recirculation height (m)
k_s = equivalent sand roughness height (m)
L_{recirc} = recirculation region length (m)
L_{roller} = roller length (m)
P = pressure (Pa)
R_{xx} = normalized auto-correlation function
S_o = bed slope (–)
T_{recirc} = recirculation region duration (s)
T_{roller} = breaking roller duration (s)
T_{toe} = roller toe passage time (s)
T_{vx} = integral time scale of longitudinal velocity component (s)
T_{vy} = integral time scale of transverse velocity component (s)
T_{vz} = integral time scale of vertical velocity component (s)
t = time (s)
U = bore celerity (m s^{-1})
V_{recirc} = maximum recirculation velocity (m s^{-1})
V_x = longitudinal velocity component (m s^{-1})
V_y = transverse velocity component (m s^{-1})
V_z = vertical velocity component (m s^{-1})
V_1 = inflow velocity (m s^{-1})
V_2 = conjugate flow velocity (m s^{-1})
v = velocity fluctuation (m s^{-1})
v_x = longitudinal velocity fluctuation (m s^{-1})
v_y = transverse velocity fluctuation (m s^{-1})
v_z = vertical velocity fluctuation (m s^{-1})
v_x' = longitudinal velocity fluctuation root mean square (m s^{-1})
v_y' = transverse velocity fluctuation root mean square (m s^{-1})
v_z' = vertical velocity fluctuation root mean square (m s^{-1})
x = longitudinal distance along the channel bottom (m)
y = transverse distance (m)
z = vertical elevation (m) above the invert
μ = dynamic viscosity (Pa.s) of water
θ = channel slope
ρ = water density (m^3 s^{-1})
σ = surface tension (N m^{-1})
τ = time lag (s)

References

Barré de Saint Venant, A. J. C. (1871). Théorie et Equations Générales du Mouvement Non Permanent des Eaux, avec Application aux Crues des Rivières et à l'Introduction des Marées dans leur Lit (2ème Note). *Comptes Rendus des séances de l'Académie des Sciences*, Paris, France, Séance 17 July 1871, *73*, 237–240.

Benet, F., & Cunge, J. A. (1971). Analysis of experiments on secondary undulations caused by surge waves in trapezoidal channels. *Journal of Hydraulic Research*, *9*(1), 11–33.

Chanson, H. (2010). Unsteady turbulence in tidal bores: Effects of bed roughness. *Journal of Waterway, Port, Coastal, and Ocean Engineering, ASCE*, *136*, 247–256. doi:10.1061/(ASCE)WW.1943-5460.0000048

Chanson, H. (2011). *Tidal bores, Aegir, Eagre, Mascaret, Pororoca: theory and observations*. Singapore: World Scientific.

Chanson. H. (2012). Momentum considerations in hydraulic jumps and bores. *Journal of Irrigation and Drainage Engineering, ASCE*, *138*, 382–385. doi:10.1061/(ASCE)IR.1943-4774.0000409

Chanson, H., & Docherty, N. J. (2012). Turbulent velocity measurements in open channel bores. *European Journal of Mechanics B/Fluids*, *32*, 52–58. doi:10.1016/j.euromechflu.2011.10.001

Chanson, H., Reungoat, D., Simon, B., & Lubin, P. (2011). High-frequency turbulence and suspended sediment concentration measurements in the Garonne River tidal bore. *Estuarine Coastal and Shelf Science*, *95*, 298–306. doi:10.1016/j.ecss.2011.09.012

Hinze, J. O. (1975). *Turbulence* (2nd ed.). New York: McGraw-Hill.

Hornung, H. G., Willert, C., & Turner, S. (1995). The flow field downstream of a hydraulic jump. *Journal of Fluid Mechanics*, *287*, 299–316.

Khezri, N., & Chanson, H. (2012). Inception of bed load motion beneath a bore. *Geomorphology*, *153–154*, 39–47. doi:10.1016/j.geomorph.2012.02.006

Koch, C., & Chanson, H. (2009). Turbulence measurements in positive surges and bores. *Journal of Hydraulic Research, IAHR*, *47*(1), 29–40. doi:10.3826/jhr.2009.2954

Lewalle, J., & Ashpis, D. E. (2004). Estimation of time scales in unsteady flows in a turbomachinery rig. NASA/TM-2004-209452, 42 pages.

Liggett, J. A. (1994). *Fluid Mechanics*. New York: McGraw-Hill.

Mouazé, D., Chanson, H., & Simon, B. (2010). Field measurements in the tidal bore of the Sélune River in the Bay of Mont Saint Michel (September 2010). Hydraulic Model Report No. CH81/10, School of Civil Engineering, The University of Queensland, Brisbane, Australia, 72 pages.

Murzyn, F., & Chanson, H. (2009). Free-surface fluctuations in hydraulic jumps: Experimental observations. *Experimental Thermal and Fluid Science*, *33*, 1055–1064. doi:10.1016/j.expthermflusci.2009.06.003

Murzyn, F., Mouazé, D., & Chaplin, J. R. (2007). Air-water interface dynamic and free surface features in hydraulic jumps. *Journal of Hydraulic Research*, *45*, 679–685.

Reungoat, D., Chanson, H., & Caplain, B. (2014). Sediment processes and flow reversal in the undular tidal bore of the Garonne River (France). *Environmental Fluid Mechanics*, *14*, 591–616. doi:10.1007/s10652-013-9319-y.

Richards, G. L., & Gavrilyuk, S. L. (2013). The classical hydraulic jump in a model of shear shallow-water flows. *Journal of Fluid Mechanics*, *725*, 492–521. doi:10.1017/jfm.2013.174.

Simpson, J. H., Fisher, N. R., & Wiles, P. (2004). Reynolds stress and TKE production in an estuary with a tidal bore. *Estuarine, Coastal and Shelf Science*, *60*, 619–627.

Tessier, B., Archer, A. W., Lanier, W. P., & Feldman, H. R. (1995). Comparison of ancient tidal rhythmites (Carboniferous of Kansas and Indiana, USA) with modern analogues (the Bay of Mont-Saint-Michel, France). *Special Publication - International Association of Sedimentologists*, *24*, 259–271.

Tricker, R. A. R. (1965). *Bores, Breakers, Waves and Wakes*. New York: American Elsevier.

Valiani, A. (1997). Linear and angular momentum conservation in hydraulic jump. *Journal of Hydraulic Research*, *35*, 323–354.